Asian Journal of Chemistry; Vol. 34, No. 1 (2022), 85-92

ASIAN JOURNAL OF CHEMISTRY

https://doi.org/10.14233/ajchem.2022.23441

Fabrication of Minerals Substituted Hydroxyapatite based Nanocomposite Coating on Titanium: Physico-Chemical and *in vitro* Biological Evaluations

DHARMAN GOVINDARAJ and MARIAPPAN RAJAN*

Biomaterials in Medicinal Chemistry Lab, Department of Natural Products Chemistry, School of Chemistry, Madurai Kamaraj University, Madurai-625021, India

*Corresponding author: E-mail: rajanm153@gmail.com

Received: 28 July 2021; *Accepted*: 14 September 2021; *Published online*: 16 December 2021; AJC-20622

The search of orthopedic metallic implants which facilitate osteoconductivity and mitigate bacterial contamination has received substantial care to ensure long-term problems in the biomedical sector. Current research studies electrophoretic deposition of gelatin (Gel)@minerals (Ce, Mg, Zn) substituted hydroxyapatite (MHA2)-halloysite nanotube (HNT)-single-walled carbon nanotubes (SWCNT) (Gel@MHA2-HNT-SWCNT) nanocomposite coatings on the surface of titanium plate. Coated samples were characterized by FTIR, XRD and SEM-EDX techniques. Furthermore, antimicrobial, hemolysis and cell viability studies of coating materials and their findings show the bacteriostatic activity, hemocompatibility and more viable cells, respectively. Overall, the *in vitro* experiments have shown that Gel@MHA2-HNT-SWCNT nanocomposite coating on titanium enhanced the biocompatible efficiency, suggesting that Gel@MHA2-HNT-SWCNT coated titanium is a potential implant substrate for orthopedic implants.

Keywords: Bone, Gelatin, Nanocomposite, Implant, Osteoblast compatibility.

INTRODUCTION

The production of bone devices in the healthcare sector is a significant study motif since they have been used to substitute different organs or portions of the patient's body [1]. Due to superior characteristics, strong corrosion resistance and cyto-compatible properties, titanium based devices are gaining access to a broad range of medical applications [2]. Given the success of titanium, there is broad potential for developing its useful characteristics for a clinical field such as accelerated fracture healing, joint contact with the implant and enhancing prosthetics' cytocompatibility for their long-term use, durable biocompatible bioceramics are typically coated on it [3].

In the category of biocompatible coating materials, hydroxyapatite [$Ca_{10}(PO_4)_6(OH)_2$] (HA) has fascinating characteristics, especially as bioactivity, good bonding capacity with native tissue formation and longer osteoconductivity [4]. Conversely, pristine hydroxyapatite demonstrates decreased bio-mineralization due to comparatively marginal bio-resorption and bacterial reduction failure. Biologically active mineral ions incorporated in pristine hydroxyapatite, the above mentioned listed difficulties can be resolved and the physico-chemical and biochemical characteristics can be enhanced for good clinical use [5].

Zinc is an important trace component in the human body and enhances bone formation [6]. Magnesium is found in bone minerals and believed to be an appropriate trace ingredient in teeth and bones [7]. In contrast with other mineral ions, cerium ions were used as antimicrobial drugs in pharmaceutical goods for several years due to high protection and a wide spectrum of antimicrobial activity [8]. As biologically active mineral ions such as Zn, Mg and Ce help to control biocompatible and antimicrobial activity; it is possible to implement all biologically active components to elicit many successful physico-chemical functions of medicinal titanium implants.

In specific, hydroxyapatite (HA) and minerals substituted hydroxyapatite (MHA) have inferior mechanical characteristics and insufficient capacity, which are ineffective relative to normal human bones and contain long-term use as orthodontic and orthopedic instruments. The mechanical characteristics of MHA ceramic based substance can be further improved by the inclusion of suitable strengthening materials including

graphene oxide (GO), carbon nanotubes (SWCNT and MWCNT), halloysite nanotubes (HNTs), alumina, zirconia, *etc.* [9,10]. HNTs and SWCNT have high mechanical strength with tubular structure from these reinforcing fillers, commonly used for biological devices. The unique characteristics of HNT and SWCNT make them effective reinforcement medium for the development of nanocomposite hydroxyapatite.

The integration of complex nanocomposites inorganic compounds with polymeric materials can improve the quality of products with great prospects for improved tissue rejuvenation [11]. On the other hand, gelatin is a natural protein polymer produced from collagen hydrolysis [12]. It has a renewable substance and shows excellent cytocompatibility and degradability characteristics in biological settings. While various coating strategies are provided to manufacture composites on surgical implants, the electrophoretic deposition (EPD) approach has received much interest given its potential benefits such as high processing temperature, accessing information and coating about any sort of coating complicated shaped or translucent surface [13]. Depending on these issues, the purpose of this work is to design and analyze the biological properties of nanocomposites coating on titanium.

EXPERIMENTAL

Preparation of MHA2 nanoparticles: A standard sol-gel aided synthesis technique has been proposed for the preparation of MHA2 (Zn + Mg + Ce substituted hydroxyapatite) nanoparticles [14]. Relevant concentrations of raw materials for calcium, zinc, magnesium and cerium ions have been dissolved in double distilled water to produce solution-I. The concentration of mineral ions of zinc (0.25 M), magnesium (0.25 M) and cerium (0.25 M) in cumulative concentrations of Ca, Zn, Mg and Ce ions (1 M) were maintained. Over the next section, 0.2 M EDTA and 0.6 M $(NH_4)_2HPO_4$ were soluble in double distilled water to form solution-II. The minerals + calcium: phosphate stoichiometric ratio was set to 1.67 in all solutions. Consequently, solution-II was applied dropwise in to solution-I with vigorous stirring at room temperature for 12 h. To maintain the pH level at 11.0, sodium hydroxide solution was added. The suspension acquired was maintained for 5 h at 50 ºC, drained off the precipitate and repeatedly washed with ethanol and double distilled water. The resulting gel was dried in the hot air oven at 100 ºC for approximately 5 h and then calcinated in the furnace at 800 ºC for 4 h at a reaction temperature of 10 °C/min.

Preparation of MHA2-HNT nanoparticles: Halloysite nanotubes (HNTs, 0.2 g) were dispersed in 0.6 M $(NH_4)_2HPO_4$ solution. Minerals (Ca, Zn, Mg and Ce) solution (1 M) was added dropwise into the dispersion. Sodium hydroxide was then used to change the pH value to over 11.0. Protocols were conducted at 50 ºC under vigorous stirring. To maintain a calcium + minerals/phosphorus ratio of 1.67, the volume of Zn + Mg + Ce was the same as that of $(NH_4)_2HPO_4$ with HNT. The subsequent solution was subjected for a further 20 min to microwave radiation. This was accompanied by the separation of the precipitate substance by filtration and frequent washing with double distilled water to eliminate precursors and residues. Further, the material was dried at 120 ºC overnight. Following drying and crushing, MHA2-HNT material was obtained.

Electrophoretic deposition of MHA2 and MHA2-HNT nanoparticles: Approximately 0.6 g of MHA2 powder was added in 50 mL of 2-propanol (Himedia) for electrophoretic deposition [15]. Suspensions were ultrasonic for 10 min and left for overnight. Two drops of HCl were introduced to the suspension and the ultrasound was performed for 10 min to ensure uniform distribution. The flag-shaped platinum as an anode and the titanium plate as the cathode was soaked in the MHA2 suspension. The distance between the anode and cathode electrode was 1 cm. Electrophoretic deposition (EPD) was conducted at a voltage supply of 30 V at room temperature for 10 min. The coatings were carefully washed with methanol and dried overnight in a 50 ºC hot air oven. This procedure was same for MHA2-HNT nanoparticles coating.

Electrophoretic deposition of nanocomposites: The SWCNT (0.1 mg/mL) was ultrasonic diffusion in a combination of ethanol and double distilled water overnight and stirring for 5 h. Nanoparticles of MHA2-HNT (6 mg/mL) were suspended in ethanol for 5 h with agitation and then applied to the SWCNT solution. After 30 min, the resulting mixture was ultrasonically treated. A gelatin solution of 0.5 mg/mL was obtained by dissolving gelatin in double distilled water for 3 h at 50 ºC. Consequently, the gelatin solution was gradually introduced to the above-mentioned combination of MHA2-HNT-SWCNT and the resultant mixed suspensions were ultrasonically dispersed for 10 min and then stirred until electrophoretic deposition for 5 h. Using 30V DC power for 10 min with a titanium substrate (cathode) and platinum (anode) 1 cm separated electrophoretic deposition procedures were carried out under constant stirring. The coated samples were properly removed out of the electrophoretic deposition cell and cured sideways in the air for 24 h at room temperature. The same process also coated the MHA2-HNT-SWCNT nanocomposite without gealtin.

Physico-chemical characterization: The spectra (Shimadzu IR Trace-100 spectrometer) for the coated samples were acquired in the scanning range of 4000 cm^{-1} to 400 cm^{-1}. The powder X-ray diffractometer (D8 Advanced ECO XRD SSD160) was used for the X-ray crystallographic analysis to investigate the crystalline phase of the coated samples. The surface morphology and elemental identification of MHA2 and its nanocomposite coated titanium were carried out by scanning electron microscopy (ZEISS-EVO 18 Research, Japan) coupled with energy dispersive X-ray analyses (Bruker-X Flash 6130), respectively.

Antibacterial and hemocompatibility studies: Antibacterial and hemocompatibility of fabricated samples were prepared by following the reported protocols [16,17].

***In vitro* bioactive studies:** To evaluate the bioactivity of the coatings, the Kokubo's SBF was employed [18]. Different samples are soaked for 14 days in 50 mL of SBF at 37 ºC. And the SBF has to be refreshed every1 day. Following 14 days of immersion, the specimens were gently rinsed with distilled water and dried at 50 ºC preceding SEM and XRD analysis.

***In vitro* cell viability:** For analyzing biocompatibility of MHA2, MHA2-HNT, MHA2-HNT-SWCNT and Gel@MHA2-

HNT-SWCNT and MG63 osteoblast-like cell culture were performed at 37 ºC in an incubator having 5% CO_2 atmosphere using DMEM media (mixed with 1%, penicillin/streptomycin and 10%, FBS). After 105 cells/100 µL DMEM were seeded in 96 well plates and incubation was followed at 37 ºC, a biocompatibility assessment was performed. Once morphological cell measurements were completed, 25, 50, 75 and 100 µg/mL of the samples were separately distributed in the culture medium. MTT (200 µL) test was done using a 4 h incubation in 1 day of cell-material interaction. After the test, aged media have been removed and 200 µL of DMSO have been put into each well with a keeping of 25 min. For the measurement of solution uptake, the UV-Vis spectrometer (570 nm) was employed.

Statistical analysis: All the analysis described in this research was conducted in triplicate and the statistical results were given as an average ± standard deviation by using origin 8.5.

RESULTS AND DISCUSSION

FTIR spectra: The spectrum shows the typical absorption peaks of native hydroxyapatite recorded for MHA2 (Fig. 1b) [19]. Those peaks at 1015 cm^{-1} to 1108 cm^{-1} (ν_3 asymmetric stretching P-O), at 608 cm^{-1} (ν_4 bending vibration of O-P-O), at 549 cm^{-1} (ν_4 asymmetric bending O-P-O) and authenticate for the development of the MHA2 phase. In addition, carbonate peaks were detected at 1382 to 1465 cm^{-1}, which confirmed the fractional exchange of carbonate groups within the MHA2 phase. In addition to the above signature FTIR peaks of the MHA2 coating, the wavenumbers of the MHA2-HNT coating sample showed the typical HNT peaks at 1088 and 1014 cm^{-1}, which become due to the Si–O and O–Si–O, accordingly (Fig. 1c). In contrast, the stretching absorption peaks were detected at 3688 and 3628 cm^{-1} corresponding to the carbonyl group positioned at aluminum hydroxide. Also, the 908 cm^{-1} bending peaks are proof of the Al–OH groups in HNT. Furthermore, the peaks at 748 and 680 cm^{-1} are attributable to the Si–O asymmetric stretching in HNT. Also, the Al–O–Si group of HNT is the bending peak at 541 cm^{-1} (Fig. 1c) [20].

For all its components, *i.e.*, gelatin, MHA2-HNT and SWCNT, the FTIR spectrum for the nanocomposites displayed standard peaks with a minor change in absorption bands (Fig. 1d-e). Gelatin (as-received) has the signatures of FTIR spectra band at 1328, 1541 and 1655 cm^{-1}, reflecting the asymmetric stretching of amide III and amide II and amide I, respectively (Fig. 1a) [21]. The peaks referring to MHA2 changed from 1015 to 1042 cm^{-1} and from 1655 to 1662 cm^{-1}, the peak corresponds to gelatin (amide-III) switched (Fig. 1e). These peak significant changes can be due to gelatin electrostatic interactions with MHA2-HNT-SWCNT. The phosphate bending vibrations at 608 and 549 cm^{-1} in pure MHA2 changed to 616 and 555 cm^{-1}. These findings confirm that all components in the nanocomposite and the forming of the nanocomposite was attributed to hydrogen bonding and ionic interactions.

Crystallographic structure: Fig. 1B displays the XRD patterns of MHA2, MHA2-HNT, MHA2-HNT-SWCNT and Gel@MHA2-HNT-SWCNT nanocomposites coated Ti substrate prepared by electrophoretic deposition. The XRD patterns of plain gelatin samples revealed an amorphous structure with high, expanding characteristic peaks between 25-30º, close to Maji *et al.* [22] findings (Fig. 1a). Fig. 1b displays the XRD patterns acquired for the MHA2 coated Ti and are in fair accordance with the standard hydroxyapatite data and the JCPD card number 09-0432. However, for the MHA2 coating, the diffraction angle locations differed moderately from the standard

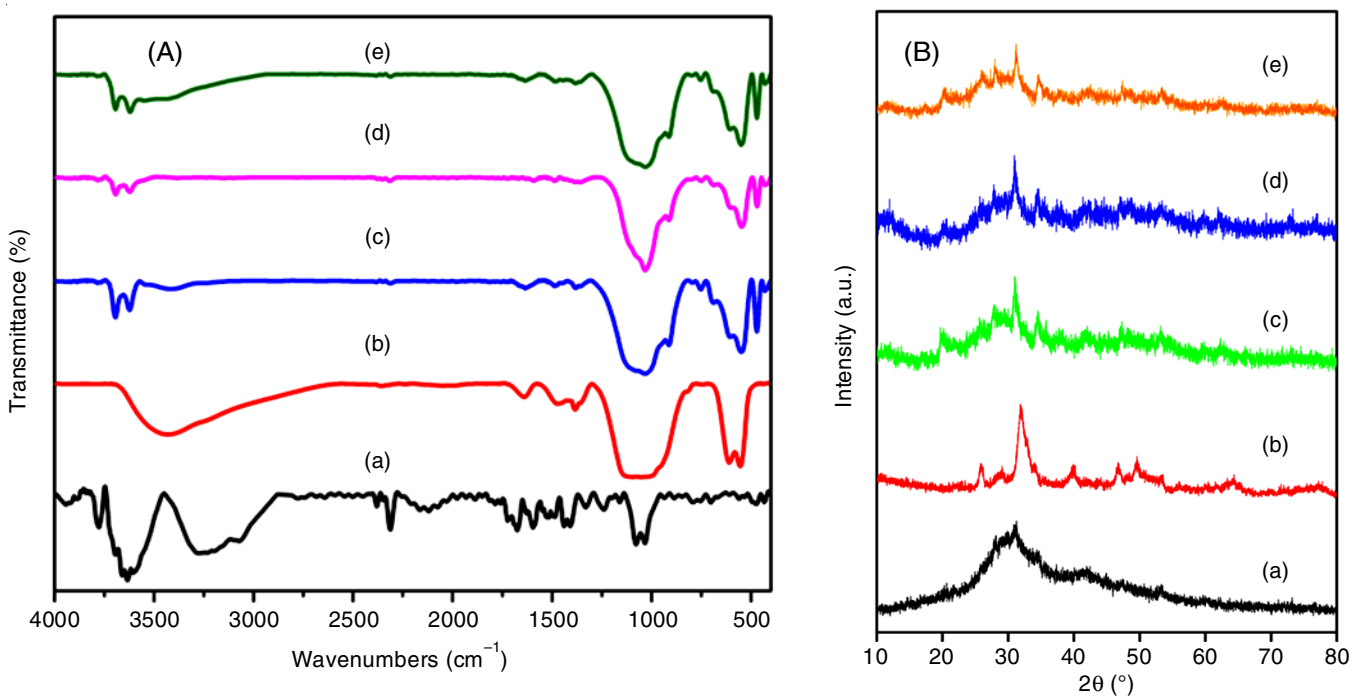

Fig. 1. (A) FTIR and (B) XRD spectrum of (a) gelatin and the electrophoretically deposited (b) MHA2, (c) MHA2-HNT, (d) MHA2-HNT-SWCNT and (e) Gel@MHA2-HNT-SWCNT coatings

hydroxyapatite pattern to the reduced 2θ positions, which may be due to the crystal structure disruption that emerged as the result of the incorporation of minerals ions into the hydroxyapatite crystals [23]. The diffraction peak positions for MHA2 coating are detected at 25º, 28º, 31º, 32º, 33º, 34º, 41º, 44º, 47º, 52º and 60º. No other supplementary points were observed for MHA2, respectively and these 2θ peaks are well consistent with prior reference studies [22,23].

Fig. 1c displays the XRD patterns acquired for the MHA2-HNT coating on Ti. As shown by Fig. 1c, in the MHA2-HNT coating diffraction, the XRD peaks of both MHA2 and HNT are detected [24]. The incorporation of the SWCNT into the MHA2-HNT structure reveals in Fig. 1d that its phase nature does not alter. Conversely, the XRD study did not observe the SWCNT points, most probably because of the disruption to their crystalline structure. It was often considered that the absence of the SWCNT peak was an indicator of the proper distribution of SWCNT in the nanocomposite [25].

Fig. 1e displays the XRD patterns of Gel@MHA2-HNT-SWCNT nanocomposite coating. Lowered intensity peaks at 28º, 31º and 34º were identified for Gel-MHA2-HNT-SWCNT, suggesting the low crystalline nature of MHA2 particles in Gel@MHA2-HNT-SWCNT nanocomposite. Nevertheless, owing to the amorphous form of gel, no phases linked to gel are found in the XRD spectrum of the nanocomposite. It is due to the reduction and rise in peak intensities may be hydrogen bond-forming, cross-linking, diffraction peak merging and chemical level balancing [26]. The XRD pattern reveals that Gel-MHA2-HNT-SWCNT coating is produced successfully at titanium.

Surface morphology and elemental composition of the coatings: The surface morphology of MHA2, MHA2-HNT, MHA2-HNT-SWCNT and Gel@MHA2-HNT-SWCNT coatings on titanium are shown in Fig. 2. The acquired SEM microstructure for the MHA2 specimen (Fig. 2a-b) shows the development of a sphere-like granular structure on the titanium implant. There were a few breaks between them, the microstructure being consistent. Besides, the HNT develops granular morphological rods in the MHA2-HNT nanoparticles (Fig. 2d-e). Fig. 2g-h demonstrates MHA2-HNT-SWCNT nanocomposite coated on titanium, which revealed the presence of nanocomposite substance granule aggregates. The coating tends to be layered gently around the titanium implant. Furthermore, the existence of SWCNT and MHA2-HNT particles was detected distinctly at higher magnification. For the Gel@MHA2-HNT-SWCNT nanocomposite coating on titanium, the SEM images (Fig. 2j-k) showed the portable packaging of component with micropores and a thick foam-like surface covering the entire substrate [27]. It was noticed that the MHA2 and MHA2-HNT coatings had a porous structure, while the SWCNT and Gel occupy these pores in the nanocomposite coatings and shaped less porous films that can be obviously shown in the higher magnified SEM pictures.

Fig. 2(c,f,i,j) showed the elements contained in the coated samples seen in the EDAX spectrum. The EDAX spectrum of the MHA2 coating on titanium is seen in Fig. 2c, which also confirms the existence of MHA2-coated layer of Ca, P, Zn, Mg, Ce and O. The EDAX spectrum of the MHA2 coating indicates that the calcium/phosphate mineral ratio is 1.3 and may signify the hydroxyapatite crystalline materials disturbance or the existence of many other CaP components as impurities. The EDAX spectrum reflecting the constituent components of the MHA2-HNT coating on titanium is seen in Fig. 2f, which indicated the distribution of Ca, P, Zn, Mg, Ce, O, Si and Al in the relative MHA2-HNT coating. Fig. 2i & j displays the EDAX results of MHA2-HNT-SWCNT and Gel@MHA2-HNT-SWCNT nanocomposite coatings, which revealed the existence of Ca, P, Zn, Mg, Ce, O, Si, Al and C (which is the basic foundation of gelatin and SWCNT), thus promoting the development of nanocomposite coatings. Conversely, for the stoichiometric hydroxyapatite, all proportions of calcium/phosphate atomic ratio are considerably smaller than 1.67, suggesting that both samples (MHA2-HNT-SWCNT (Ca/P = 1.3) and Gel@MHA2-HNT-SWCNT (Ca/P = 1.3) are apatite deficient in calcium [28]. The Ca-deficient hydroxyapatite may help to induce the new bone tissue development *in vivo* [29]. Moreover, the lack of such cations and anions confirms the purity of the coating.

***In vitro* antibacterial activity:** It was observed that the Gel@MHA2-HNT-SWCNT and MHA2-HNT-SWCNT nanocomposites coating demonstrates improved antibacterial actions towards *E. coli* in comparison to MHA2 and MHA2-HNT, which may be attributable to less low-density cell walls. The feasible *S. aureus* is inhibited mainly by nanocomposite materials. It shows more colonies than *E. coli* covered with a thick cell membrane. Also, coatings MHA2 and MHA2-HNT showed a relative inhibition in *S. aureus* and *E. coli* relative to nanocomposites (Fig. 3). It is also evident that Gel@MHA2-HNT-SWCNT coating tends to minimize bacterial attachment and demonstrates outstanding antimicrobial properties against all bacterial species, which could be a cure for periprosthetic infections.

***In vitro* hemocompatibility:** The components of MHA2, MHA2-HNT, MHA2-HNT-SWCNT and Gel@MHA2-HNT-SWCNT were analyzed. The *in vitro* hemocompatibility evaluation in animal blood at increasing doses, such as 20-100 µg/mL, which can pose a risk to a blood cell surface and hemoglobin secretion (Fig. 4). The hemolysis level spectrum is less than 2% non-hemolytic. A 2-5% is mildly hemolytic and more than 5% is hemolytic, as per the ASTM 756-00 and ISO 10 993-5 1992 reports [30]. The overall hemolytic ratio of MHA2, MHA2-HNT, MHA2-HNT-SWCNT and Gel@MHA2-HNT-SWCNT samples was seen as 2.7, 3.3, 3.8 and 3.4%, respectively. It was found that Gel@MHA2-HNT-SWCNT nanocomposite is hemocompatible with hemolysis of less than 5% at different concentrations of 20-100 µg/mL. Compare to MHA2 and MHA2-HNT nanoparticles, the MHA2-HNT-SWCNT was mildly hemolytic with regards to doses of 20-100 µg/mL, which may be attributed to the incorporation into the membrane of RBC cells of a CNT.

The inclusion of SWCNT adds to an elevated percentage of hemolysis relative to the substance protected by the MHA2, but not to a degree that can be considered harmful to the human body [31]. However, it was observed that all samples display

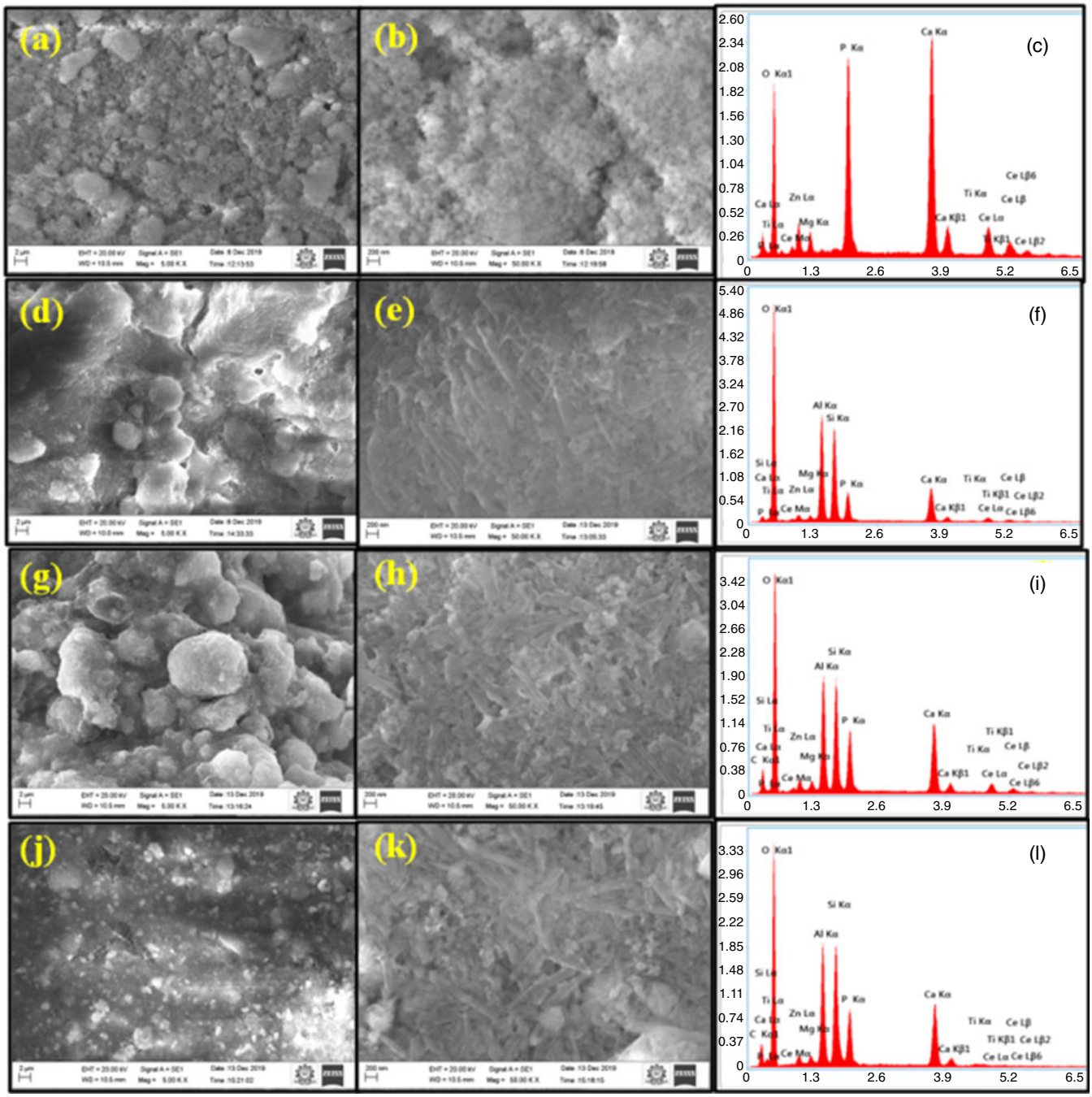

Fig. 2. SEM-EDAX images of the electrophoretically deposited MHA2 (a-c), MHA2-HNT (d-f), MHA2-HNT-SWCNT (g-i) and Gel@MHA2-HNT-SWCNT coatings (j-l)

less than 5% hemolytic behaviour and demonstrated that this Gel@MHA2-HNT-SWCNT nanocomposite is hemocompatible in character. This experiment may also be viewed as a preface analysis of the biocompatibility report. Composites of CNT and HNT clay have long been described as hemocompatible [32]. This hemocompatibility test demonstrates that the processed Gel@MHA2-HNT-SWCNT nanocomposite serves as favourable materials for biomedical applications.

***In vitro* bioactivity:** Fig. 5A shows the structure of the coated samples at 30 ºC after 14-days of immersion in SBF solution. The gelatin and SWCNT strengthened MHA2-HNT coated Ti plate encountered strong bioavailability and deposition of the apatite coating on their interfaces. The addition of gelatin and SWCNT facilitates the mineralization within the human physiological environment [33]. As seen in Fig. 5A, the amount of crystallization increased with the addition of Gel and SWCNT to MHA2-HNT. The SEM picture for the Gel@MHA2-HNT-SWCNT nanocomposite produced a thick surface supernatant substrate with a smaller percentage of voids relative to MHA2-HNT and MHA2. Fig. 5B shows the XRD patterns of the coated samples at 30 ºC after 14-days of immersion in SBF. Without some structural adjustment, the peak locations are in strong accordance with JCPDS 09-0432. Also, the nanocomposites XRD pattern after immersion in SBF

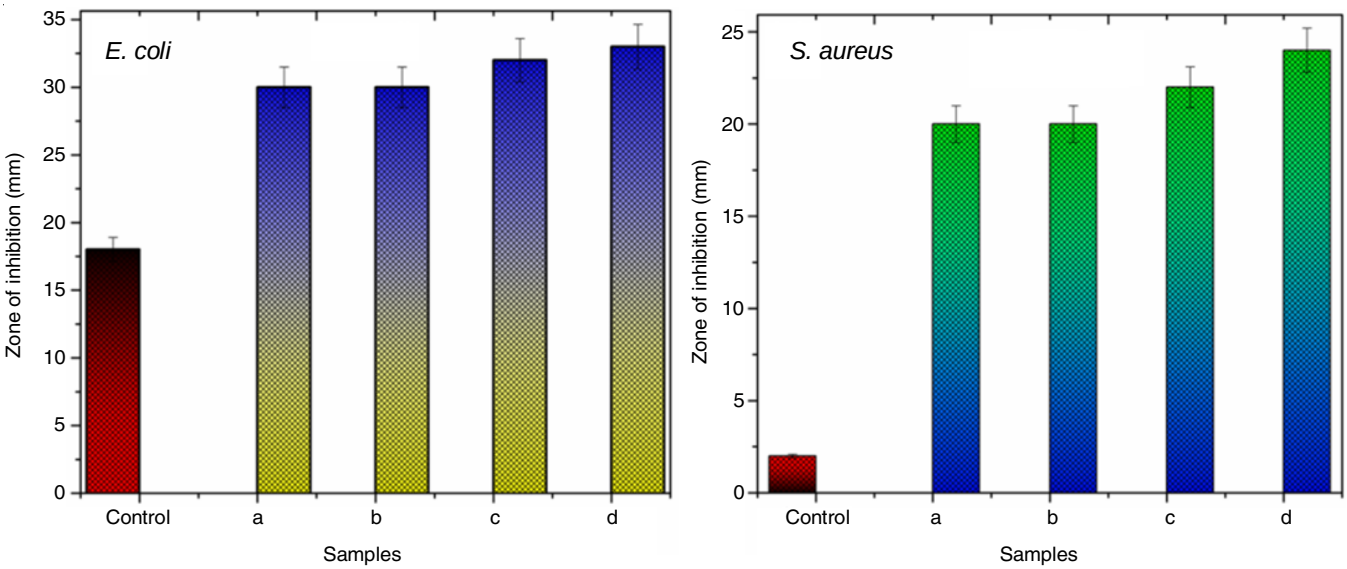

Fig. 3. Antibacterial activity of the electrophoretically deposited (a) MHA2, (b) MHA2-HNT, (c) MHA2-HNT-SWCNT and (d) Gel@MHA2-HNT-SWCNT coatings

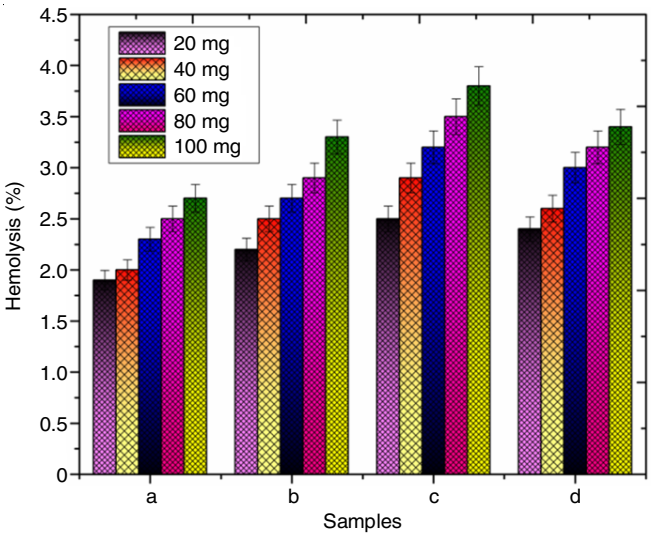

Fig. 4. Hemocompatibility assay of the electrophoretically deposited (a) MHA2, (b) MHA2-HNT, (c) MHA2-HNT-SWCNT and (d) Gel@MHA2-HNT-SWCNT coatings

displays stronger peaks contrasted with the parent and other samples (Fig. 5B). Besides, the crystalline planes (202), (112), (211) and (002) of MHA2 are attributed to the peaks identified to be at 34º, 32º, 31º and 2º. After the 14th day of immersion, the weak intense peak at 2θ = ~ 31º becomes much more intense. Moreover, Fig. 5C shows the nanocomposite-coated Ti plate's weight increased compared to parent and other composites due to the formation of apatite on the nanocomposite-coated Ti plate.

***In vitro* biocompatibility:** Fig. 6A demonstrates the cell viability of osteoblast-like cells cultivated with MHA2, MHA2-HNT, MHA2-HNT-SWCNT and Gel@MHA2-HNT-SWCNT nanocomposite samples. All samples demonstrated good cell viability with osteoblast-like cells, as all material usually hydroxyapatite, is the major inorganic component of human teeth and bones. The existence of SWCNT substances doesn't really impact the cell viability of nanocomposites. It is observed that the cell viability of all coated samples has declined with an increase in the concentration of the specimens.

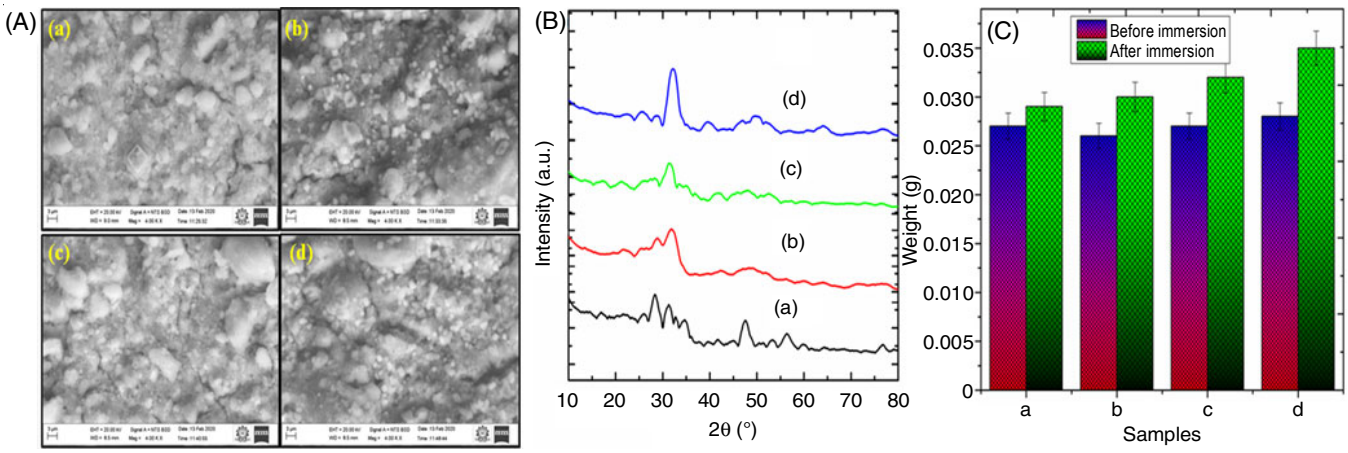

Fig. 5. (A) SEM, (B) XRD spectra and (c) weight change of the electrophoretically deposited (a) MHA2, (b) MHA2-HNT, (c) MHA2-HNT-SWCNT and (d) Gel@MHA2-HNT-SWCNT coatings after immersion in SBF for 14 days

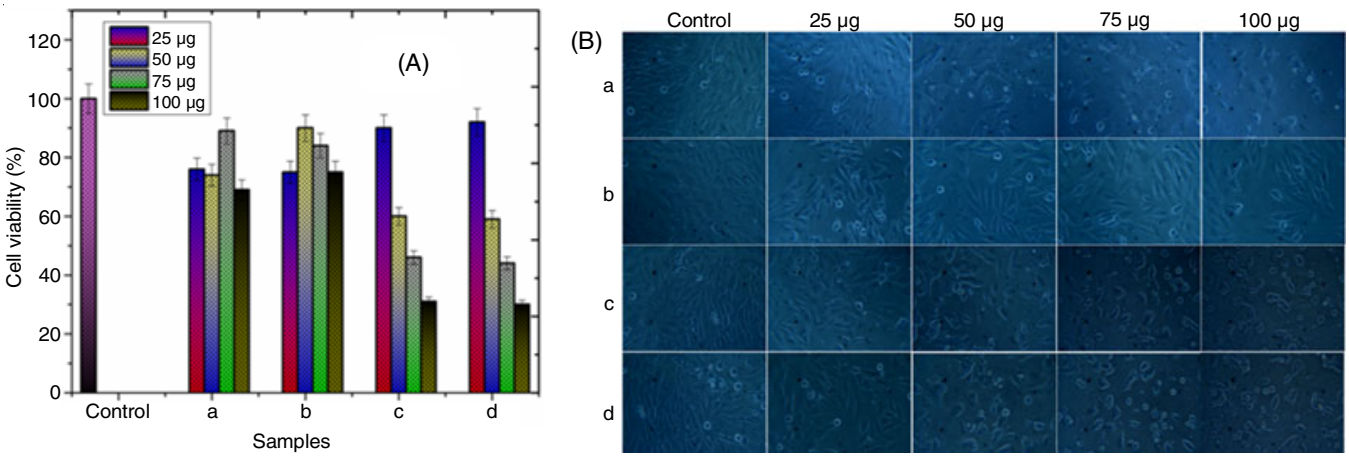

Fig. 6. (A) Cell viability and (B) optical images of osteoblast-like cells on 25-100 µg/mL concentrations of electrophoretically deposited (a) MHA2, (b) MHA2-HNT, (c) MHA2-HNT-SWCNT and (d) Gel@MHA2-HNT-SWCNT coatings for 24 h

As per the biomedical assessment of medical equipment 5: *In vitro* cytotoxicity studies (ISO 10993-5: 2009), if the substance's cell viability is less than 70%, it has a cytotoxic capacity [34]. This *in vitro* MTT evaluation thus shows that nanocomposites can be suggested for use in tissue engineering at lower doses. This was further shown by the inverted phase-contrast microscopy (Fig. 6B), which reveals a prominent cell reaction in terms of cell binding, extending over 25-100 µg/mL with the extended filament cellular proliferation while at 75-100 µg/mL, the non-viable cells possess further dead cells. The *in vitro* MTT evaluation thus shows that nanocomposites can be suggested for use in tissue engineering at lower doses.

Conclusion

To improve the biocompatibility of titanium and to enhance its biofunctional characteristics, bioactive coatings have been studied. For this reason, through electrophoretic deposition, Gel@MHA2-HNT-SWCNT coatings have been successfully applied to the titanium surface. Sphere, rod and foam-like images were identified in the morphology of MHA2, MHA2-HNT, MHA2-HNT-SWCNT and Gel@MHA2-HNT-SWCNT coatings developed by electrophoretic deposition, proving the existence of MHA2, HNT, SWCNT and Gel, respectively. Furthermore, FTIR and XRD results confirmed the formation of these phases. In addition, the 14-day mineralization analysis of the Gel@MHA2-HNT-SWCNT nanocomposite exhibits great apatite development with bone-mimicking characteristics. The outcome of hemocompatibility indicates that the Gel@MHA2-HNT-SWCNT nanocomposite is below reasonable ASTM limits and has strong consistency with blood with less than 5% of the hemolysis ratio. The antibacterial activity shows that the effective antimicrobial activity against the pathogens of *E. coli* and *S. aureus* was seen in all coated samples. Nevertheless, the inhibition zone observed for Gel@MHA2-HNT-SWCNT nanocomposite is greater than the other samples. Biocompatibility was observed for all coating as scrutinized by MTT assays, while Gel@MHA2-HNT-SWCNT demonstrated modest cytotoxicity. Therefore, better hemocompatibility, biocompatibility and increased osteogenic of the Gel@ MHA2-HNT-SWCNT nanocomposite coated implant would act as a useful applicant for developments in biomedical applications.

CONFLICT OF INTEREST

The authors declare that there is no conflict of interests regarding the publication of this article.

REFERENCES

1. M. Niinomi, *J. Mech. Behav. Biomed. Mater.*, **1**, 30 (2008); https://doi.org/10.1016/j.jmbbm.2007.07.001
2. L.C. Zhang and L.Y. Chen, *Adv. Eng. Mater.*, **21**, 1801215 (2019); https://doi.org/10.1002/adem.201801215
3. M. Regis, E. Marin, L. Fedrizzi and M. Pressacco, *MRS Bull.*, **40**, 137 (2015); https://doi.org/10.1557/mrs.2015.1
4. J. Fang, P. Li, X. Lu, L. Fang, X. Lü and F. Ren, *Acta Biomater.*, **88**, 503 (2019); https://doi.org/10.1016/j.actbio.2019.02.019
5. D. Predoi, S.L. Iconaru, M.V. Predoi, G.E. Stan and N. Buton, *Nanomaterials*, **9**, 1295 (2019); https://doi.org/10.3390/nano9091295
6. B.M. Hidalgo-Robatto, M. López-Álvarez, A.S. Azevedo, J. Dorado, J. Serra, N.F. Azevedo and P. González, *Surf. Coat. Technol.*, **333**, 168 (2018); https://doi.org/10.1016/j.surfcoat.2017.11.006
7. M. Nabiyouni, T. Brückner, H. Zhou, U. Gbureck and S.B. Bhaduri, *Acta Biomater.*, **66**, 23 (2018); https://doi.org/10.1016/j.actbio.2017.11.033
8. D.S. Morais, S. Fernandes, P.S. Gomes, M.H. Fernandes, P. Sampaio, M.P. Ferraz, J.D. Santos, M.A. Lopes and N. Sooraj Hussain, *Biomed. Mater.*, **10**, 055008 (2015); https://doi.org/10.1088/1748-6041/10/5/055008
9. R. Barabás, E. de Souza-Ávila, L.O. Ladeira, L.M. Antônio, R. Tötös, D. Simedru, L. Bizo and O. Cadar, *Arab. J. Sci. Eng.*, **45**, 219 (2020); https://doi.org/10.1007/s13369-019-04058-4
10. M.A. Afzal, P. Kesarwani, K.M. Reddy, S. Kalmodia, B. Basu and K. Balani, *Mater. Sci. Eng. C*, **32**, 1164 (2012); https://doi.org/10.1016/j.msec.2012.03.003
11. N. Shao, J. Guo, Y. Guan, H.H. Zhang, X. Li, X. Chen, D. Zhou and Y. Huang, *Biomacromolecules*, **19**, 3637 (2018); https://doi.org/10.1021/acs.biomac.8b00707
12. H.W. Kwak, J.E. Kim and K.H. Lee, *React. Funct. Polym.*, **136**, 86 (2019); https://doi.org/10.1016/j.reactfunctpolym.2018.12.020
13. X. Pang, T. Casagrande and I. Zhitomirsky, *J. Colloid Interface Sci.*, **330**, 323 (2009); https://doi.org/10.1016/j.jcis.2008.10.070

14. K. Ishikawa, E. Garskaite and A. Kareiva, *J. Sol-Gel Sci. Technol.*, **94**, 551 (2020); https://doi.org/10.1007/s10971-020-05245-8
15. G. Sun, J. Ma and S. Zhang, *Mater. Sci. Eng. C*, **39**, 67 (2014); https://doi.org/10.1016/j.msec.2014.02.023
16. N. Sakthiguru and M.A. Sithique, *Int. J. Biol. Macromol.*, **152**, 873 (2020); https://doi.org/10.1016/j.ijbiomac.2020.02.289
17. E. Kenawy, A.M. Omer, T.M. Tamer, M.A. Elmeligy and M.M. Eldin, *Int. J. Biol. Macromol.*, **139**, 440 (2019); https://doi.org/10.1016/j.ijbiomac.2019.07.191
18. T. Kokubo and H. Takadama, *Biomaterials*, **27**, 2907 (2006); https://doi.org/10.1016/j.biomaterials.2006.01.017
19. A.M. Fathi, M.K. Ahmed, M. Afifi, A.A. Menazea and V. Uskokoviæ, *ACS Biomater. Sci. Eng.*, **7**, 360 (2021); https://doi.org/10.1021/acsbiomaterials.0c01105
20. N.S. Radda'a, W.H. Goldmann, R. Detsch, J.A. Roether, L. Cordero-Arias, S. Virtanen and A.R. Boccaccini, *Surf. Coat. Technol.*, **327**, 146 (2017); https://doi.org/10.1016/j.surfcoat.2017.07.048
21. H. Kim, H. Hwangbo, Y. Koo and G. Kim, *Int. J. Mol. Sci.*, **21**, 3401 (2020); https://doi.org/10.3390/ijms21093401
22. K. Maji, S. Dasgupta, K. Pramanik and A. Bissoyi, *Mater. Sci. Eng. C*, **86**, 83 (2018); https://doi.org/10.1016/j.msec.2018.02.001
23. X. Yin, L. Yan, D.J. Hao, S. Liu, M. Yang, B. He and Z. Liu, *Int. J. Pharm.*, **582**, 119303 (2020); https://doi.org/10.1016/j.ijpharm.2020.119303
24. M. Chozhanathmisra, K. Pandian, D. Govindaraj, P. Karthikeyan, L. Mitu and R. Rajavel, *J. Chem.*, **2019**, 7472058 (2019); https://doi.org/10.1155/2019/7472058
25. S.A. Xavier and U. Vijayalakshmi, *Colloids Surf. B Biointerfaces*, **171**, 186 (2018); https://doi.org/10.1016/j.colsurfb.2018.06.058
26. J. Hou, Y. Wang, H. Xue and Y. Dou, *Polymers*, **10**, 1032 (2018); https://doi.org/10.3390/polym10091032
27. F.M. Ghorbani, B. Kaffashi, P. Shokrollahi, E. Seyedjafari and A. Ardeshirylajimi, *Carbohydr. Polym.*, **118**, 133 (2015); https://doi.org/10.1016/j.carbpol.2014.10.071
28. B. Aellach, A. Ezzamarty, J. Leglise, C. Lamonier and J.F. Lamonier, *Catal. Lett.*, **135**, 197 (2010); https://doi.org/10.1007/s10562-010-0282-7
29. E.M. Mahmoud, M. Sayed, A.M. El-Kady, H. Elsayed and S.M. Naga, *Int. J. Biol. Macromol.*, **165**, 1346 (2020); https://doi.org/10.1016/j.ijbiomac.2020.10.014
30. M. Fedel, *J. Carbon Res.*, **6**, 12 (2020); https://doi.org/10.3390/c6010012
31. U. Anjaneyulu, V.K. Swaroop and U. Vijayalakshmi, *RSC Adv.*, **6**, 10997 (2016); https://doi.org/10.1039/C5RA21479C
32. S. Kar, P. Nandy, R. Basu and S. Das, *Mol2Net*, **1**, 1 (2015); https://doi.org/10.3390/MOL2NET-1-d002
33. X. Li, J. Lan, M. Ai, Y. Guo, Q. Cai and X. Yang, *Colloids Surf. B Biointerfaces*, **123**, 753 (2014); https://doi.org/10.1016/j.colsurfb.2014.10.026
34. O. Jung, R. Smeets, P. Hartjen, R. Schnettler, F. Feyerabend, M. Klein, N. Wegner, F. Walther, D. Stangier, A. Henningsen, C. Rendenbach, M. Heiland, M. Barbeck and A. Kopp, *Int. J. Mol. Sci.*, **20**, 255 (2019); https://doi.org/10.3390/ijms20020255